

The Vertical Structure and Ultraviolet Spectrum of Accretion Disks Heated by Internal Dissipation in Active Galactic Nuclei

Mark W. Sincell

Department of Physics MC 704
The University of Illinois at Urbana-Champaign
1110 W. Green Street
Urbana, IL 61801-3080

Julian H. Krolik

Department of Physics & Astronomy
The Johns Hopkins University
Baltimore, MD 21218

ABSTRACT

We present an improved calculation of the vertical structure and ultraviolet spectrum of a dissipative accretion disk in an AGN. We calculate model spectra in which the viscous stress is proportional to the total pressure, the gas pressure only and the geometric mean of the radiation and gas pressures (cf. Laor & Netzer 1989: LN89). As a result of a more complete treatment of absorptive opacity, we find greater overall spectral curvature than did LN89, as well as larger amplitudes in both the Lyman and HeII photoionization edges. The local black body approximation is not a good description of the near UV spectrum. With relativistic corrections (appropriate to non-rotating black holes) included, we find that the near UV spectrum hardens with increasing \dot{m}/m_8 (\dot{m} is the accretion rate in Eddington units, m_8 the black hole mass in units of $10^8 M_\odot$). The near UV spectrum is consistent with observations if $\dot{m}m_8^{-1} \sim 10^{-3}$, but disks this cold would have large, and unobserved, absorption features at the Lyman edge. The edge amplitude is reduced when \dot{m}/m_8 is larger, but then the near-UV slope is too hard to match observations. We conclude that models in which conventional disks orbit non-rotating black holes do not adequately explain UV continuum production in AGN.

1. Introduction

The optical and UV emission of radio-quiet active galactic nuclei (AGNs) is dominated by a quasi-thermal component, the “Big Blue Bump” (Shields 1978, Malkan & Sargent 1982, Malkan 1983). The Big Blue Bump is usually interpreted as thermal emission from a geometrically thin, optically thick, accretion disk around a massive black hole (Malkan 1983, Sun & Malkan 1989, Laor & Netzer 1989: LN89). There are two general reasons for this belief. First, if the accreting gas has any angular momentum far from the black hole, it will collapse to a disk as it falls into the gravitational potential of the hole. Second, the effective temperature of radiation from optically thick gas accreting onto a 10^8 solar mass black hole at the Eddington accretion rate is roughly $T_{eff} \sim 10^5$ K. Black body emission at 10^5 K peaks in the optical and UV bands. Unfortunately, theoretical models of accretion disk spectra do not agree with the observed optical-UV spectra of AGNs.

A benchmark calculation of the vertical structure and optical-UV spectrum of an accretion disk around a massive black hole was performed by LN89 (see also Laor, Netzer & Piran 1990 and Laor 1990). They calculated the radial structure of the disk for three different viscosity prescriptions and computed the corresponding emergent spectra with a semi-analytic approximation to the radiative transfer equation. The predicted slope of the near UV spectrum ($\alpha_n \sim 0.1$, where $F(\nu) \propto \nu^{\alpha_n}$) was larger than the mean near UV spectral index for a sample of ~ 100 AGNs ($\alpha_{obs} \sim -0.5$, Laor 1990). LN89 also predicted that Lyman edge features, both in absorption and emission, should generally be present in accretion disk spectra. However, Lyman edge features have only been detected in a few AGNs (Antonucci, Kinney & Ford 1989, Koratkar, Kinney & Bohlin 1992).

Since the work of LN89, the sophistication of numerical models of AGN accretion disks has increased dramatically, without a corresponding improvement in fits to the observed UV spectra. These models can be broadly divided into two groups: those which compute the UV spectrum using the diffusion approximation (Ross, Fabian & Mineshige 1992, Shimura & Takahara 1993, Dörrer, *et al.* 1996) and those which explicitly solve the radiative transfer equations (Hubeny & Hubeny 1997, Blaes & Agol 1996, Storzer, Hauschildt & Allard 1994).

In this paper, we present a calculation of the UV spectra of accretion disks around massive non-rotating black holes using the method developed by Sincell & Krolik (1997). We solve the frequency- and angle-dependent radiative transfer equation with a variable Eddington factor method (Auer & Mihalas 1970). We assume LTE level populations and neglect Comptonization. The gas temperature is determined by balancing viscous and radiative heating with radiative cooling and the density is determined by hydrostatic equilibrium. The local disk spectra are then added together, including Doppler boosting by the rotation of the disk and the redshift caused by propagation out of the potential well of the black hole, to form the observed integrated disk spectrum.

2. Method

The emergent flux from one face of a geometrically thin Keplerian disk around a black hole is

$$Q_{dis} = \frac{3GM\dot{M}}{8\pi R^3} \left(\frac{Q_{NT}}{B_{NT}C_{NT}^{1/2}} \right), \quad (1)$$

independent of the viscosity. The relativistic correction factors Q_{NT} , B_{NT} , and C_{NT} are taken from the standard references (Novikov & Thorne 1973, Page & Thorne 1974), and apply to accretion disks around non-rotating (Schwarzschild) black holes.

The surface density required to support a given accretion rate is determined by relating the vertically-averaged r - ϕ component of the stress tensor to local physical conditions. The conventional *ansatz* for doing this is the “ α ”-model introduced by Shakura & Sunyaev (1973), in which this component of the stress is taken to be a dimensionless number α_{SS} times the vertically-averaged pressure. However, as Shakura & Sunyaev (1976) showed, this model is thermally unstable when, as commonly occurs, the disk pressure is dominated by radiation.

In the absence of a compelling physical argument for any particular viscosity prescription, we follow LN89 and investigate three different stress prescriptions. We calculate the disk surface mass density assuming that the stress tensor is proportional to the total (gas plus radiation) pressure, the gas pressure and the geometric mean of the radiation and gas pressures. The second and third models are thermally stable. We choose $\alpha_{SS} = 0.1$, but the results depend only very weakly on the value of this number.

Under these assumptions, the (half) surface mass density at a given radius $r = R/R_s$, where $R_s = 2GM/c^2$ is the Schwarzschild radius, is

$$\Sigma_T = 0.723\alpha_{SS}^{-1}\dot{m}^{-1}r^{3/2} \left(\frac{B_{NT}^3 C_{NT}^{1/2} E_{NT}}{A_{NT}^2 Q_{NT}} \right) \text{ gm cm}^{-2}. \quad (2)$$

for $t_{r\phi} \sim P_r + P_g$ (the P_t case),

$$\Sigma_T = 5.63 \times 10^3 \alpha_{SS}^{-8/9} \dot{m}^{1/9} m_8^{-1/9} r^{1/3} \left(\frac{B_{NT} C_{NT}^{1/2} E_{NT}^{4/9}}{A_{NT}^{8/9} Q_{NT}^{1/9}} \right) \text{ gm cm}^{-2} \quad (3)$$

for $t_{r\phi} \sim (P_r P_g)^{1/2}$ (the P_m case) and

$$\Sigma_T = 1.27 \times 10^7 \alpha_{SS}^{-4/5} \dot{m}^{3/5} m_8^{1/5} r^{-3/5} \left(\frac{C_{NT}^{1/2} Q_{NT}^{3/5}}{B_{NT}^{3/5} D_{NT}^{4/5}} \right) \text{ gm cm}^{-2} \quad (4)$$

for $t_{r\phi} \sim P_g$ (the P_g case). In these expressions we introduce \dot{m} , the accretion rate in units of the Eddington critical accretion rate assuming the Schwarzschild efficiency of 0.057, and m_8 , the mass of the central black hole in units of 10^8 solar masses (*e.g.*, SK97). The relativistic correction factors are taken from Novikov & Thorne (1973) and Riffert & Herold (1995).

To find the local heating rate per unit mass, we assume that at any given radius the heating rate is independent of position. It is then

$$\frac{dQ}{d\Sigma} = \frac{2Q_{dis}}{\Sigma_T}, \quad (5)$$

where the factor of two reflects the fact that Σ_T is the total surface mass density of the disk and we are calculating the flux from only one face of the disk.

We determine the vertical structure and UV spectrum of the disk by solving the coupled differential equations describing the transfer of radiation, hydrostatic equilibrium, and the relation between optical depth and the vertical coordinate, subject to the local constraints of thermal equilibrium and charge conservation. We include electron scattering, bremsstrahlung and HI, HeI and HeII photoionization opacities and the corresponding continuum cooling processes. We neglect all line opacities and emissivities. A detailed description of the computational method is presented in SK97.

In order to calculate the spectrum of a conventional disk, we have made two changes to the method described in SK97. First, the local heating rate is determined by viscous heating (eq. 5). In the present paper, we neglect irradiation of the disk. Second, the boundary conditions on the radiation flux and the gas pressure have been changed. The gas pressure at the upper edge of the disk is set to a small fraction of the total central pressure. The radiation flux is set to zero at the disk midplane.

3. Results

3.1. Vertical Structure of the Accretion Disk

The analytic solution used by LN89 for the gas density (their equations 13, along with their assumption of constant density as a function of altitude) and temperature (as expressed in their equation 25) is in good agreement with our calculation because electron scattering dominates the flux weighted mean opacity. A typical example of the results of

a vertical structure calculation is shown in fig. 1. The dashed lines are the gas density and temperature profiles used by LN89. The gas density is constant near the midplane of the disk, as expected for a radiation pressure dominated disk, but drops rapidly above $\Sigma \sim 100 \text{ gm cm}^{-2}$. The LN89 estimate of the gas density at the midplane is about a factor of two smaller than the actual central density and about an order of magnitude larger than the density at $\Sigma = 1 \text{ gm cm}^{-2}$. The discrepancy at the midplane is due to the Riffert & Herrold (1995) corrections to the expression for the vertical gravity in the relativistic portion of a thin disk, which were not included in LN89. The numerical value for the midplane density agrees with the LN89 value to within a few percent when we use the same expression for the vertical gravity as they used. The gas temperature estimate of LN89 is a good approximation to the true profile at large optical depths, but the more accurate treatment gives temperatures which are about 10% higher near the top of the disk.

3.2. Accretion Disk Spectra

Despite the close agreement between the gas pressure and temperature profiles, our predicted spectrum is quite different from the one found by LN89. The reason for the discrepancy is that the LN89 calculation of the emergent spectrum is accurate only if electron scattering dominates the opacity at *all* frequencies. They define the mass column Σ_{ph} of the UV photosphere at ν by setting the effective optical depth of the photosphere

$$\tau_{ph} = \left(\frac{\kappa_{a,\nu}}{\kappa_{a,\nu} + \kappa_{es}} \right)^{1/2} \kappa_{es} \Sigma_{ph} = \frac{2}{3}. \quad (6)$$

When $\kappa_{a,\nu} \gtrsim \kappa_{es}$, this expression gives the erroneous result that $\tau_{ph} = \kappa_{es} \Sigma_{ph}$, rather than the correct optical depth, $\tau_{ph} = \kappa_{a,\nu} \Sigma_{ph}$. As a result, this prescription overestimates Σ_{ph} by a factor $\kappa_{a,\nu} / \kappa_{es}$.

Because the temperature increases with increasing Σ , this method overestimates the photospheric temperature, and the observed flux at ν , when $\kappa_{a,\nu} \gtrsim \kappa_{es}$. We find that the absorptive opacity dominates several significant frequency ranges—well below the Lyman edge (where free-free opacity is important) and just above the HeII edge (HeII photoionization opacity), even though electron scattering dominates the flux-weighted opacity. Therefore, the largest differences between our calculation and LN89 occur in these frequency ranges.

Our improvements in the radiative transfer calculation result in three changes to the predicted spectrum of an accretion disk (fig. 2). First, we find that the slope of the

non-ionizing continuum is much harder than predicted by LN89. The free-free opacity $\kappa_{ff} \gtrsim \kappa_{es}$ well below the Lyman edge, so the mass column of the photosphere increases with frequency ($\kappa_{ff} \propto \nu^{-3}$, Rybicki & Lightman 1979). This results in a rapid increase in the flux density with frequency because radiation from higher frequencies comes from hotter gas. In contrast, the LN89 prescription results in a nearly constant Σ_p in this frequency range and a much weaker frequency dependence for the flux. Second, the amplitudes of the spectral features are underestimated by the LN89 model. The opacity jump across the Lyman edge is large in both models but, for the reasons outlined above, LN89 underestimate the corresponding change in photospheric temperature because $\kappa_{a,\nu} \gtrsim \kappa_{es}$. Third, the continuum flux above the HeII edge is overestimated by LN89. The HeII photoionization opacity is much larger than κ_{es} at $r \lesssim 10$, where most of the high frequency flux is formed, which causes the LN89 approach to overestimate the photospheric temperature.

The surface mass density of the disk is smallest for the P_t case and largest for the P_g case (eqs. 2 - 4). Although the difference in Σ_T can be many orders of magnitude, we find that the spectral changes are comparatively small (fig. 5). The gas density increases with Σ , so the bound-free opacity of the P_t case is much smaller than either the P_m or P_g cases. Compared to the other cases, the flux above the HeII edge is about a factor of ten larger in the P_t case, with a corresponding decrease of a factor of two in flux below the Lyman edge. The flux between these frequencies is nearly the same in all three cases. The shift of flux from low to high frequencies results in smaller edge features for the P_t case.

In figures 3 and 4 we plot the spectra of the standard accretion disk as a function of m_8 for fixed \dot{m} and as a function of \dot{m} for fixed m_8 , respectively. In order to illustrate the effects of variations in these parameters, we fix the viscosity prescription and use the thermally stable P_m case. Although there is continuous curvature to the spectra, they can be characterized by three parameters: the near (α_n) and far (α_f) UV spectral indices and the amplitude of the Lyman edge feature (A_l). We define the spectral indices as

$$\alpha_{n,f} = \frac{\log F(\nu_2) - \log F(\nu_1)}{\log \nu_2 - \log \nu_1}, \quad (7)$$

where $\log \nu_1 = 14.8$ and $\log \nu_2 = 15.5$ for α_n , and $\log \nu_1 = 15.5$ and $\log \nu_2 = 16.0$ for α_f . The amplitude of the Lyman edge feature is defined as the ratio of the fluxes just above and below the edge. This quantity is less than one for absorption edges and larger than one for emission edges.

The shape of the spectrum depends primarily on the ratio of the accretion rate to the central mass, \dot{m}/m_8 (see table 1). This quantity determines the effective temperature scale of the disk because $T_{eff} \propto Q_{dis}^{1/4} \propto (\dot{m}/m_8)^{3/4}$. We find that the near UV spectral index hardens from $\alpha_n \simeq -0.6$ for $\dot{m}/m_8 = 0.001$ and $m_8 = 27.0$ to $\alpha_n \simeq 0.4$ for $\dot{m}/m_8 = 0.1$

and $m_8 = 0.27$. For the same range of \dot{m}/m_8 , the far UV spectral index increases from $\alpha_f \sim -\infty$ (no flux above the Lyman edge) to $\alpha_f \simeq -1.2$ and the amplitude of the Lyman edge increases from $A_l \sim 0$ (no flux above the Lyman edge) to $A_l \simeq 1.6$. The near UV spectral index is also weakly dependent on the disk luminosity ($\propto \dot{m}m_8$) so that the spectrum softens slightly with increasing disk luminosity. No appreciable emission is seen above the HeII edge in any of the disks. Only in the hottest case ($\dot{m} = 0.3, m_8 = 2.7$) is any emission seen at those frequencies.

Although the near UV spectral index of the hotter disks is near the canonical $\alpha_n = 1/3$ power law, appropriate for a Newtonian disk (*e.g.*, Pringle 1981), this is a coincidence caused by two competing effects. On the one hand, we find that the near-UV spectrum of an individual ring is significantly harder than a black body at its effective temperature. On the other hand (as pointed out by LN89), the general relativistic corrections to the disk structure equations soften the disk-integrated spectrum by making the dependence of temperature on radius shallower.

3.3. Check of the Model Assumptions

The computed gas temperature and pressure profiles also allow us to make an *a posteriori* check of our model assumptions: LTE level populations and no Comptonization.

Comptonization will change the observed disk spectrum if the Compton opacity is larger than the absorptive opacity and the Compton y -parameter, defined as $y \equiv 4kT/(m_e c^2) \max(\tau_T, \tau_T^2)$ (Rybicki and Lightman 1979), is greater than unity. In the present context, the relevant Compton optical depth is the optical depth from the photosphere to the disk surface, so $\tau_T = \Sigma_{ph} \kappa_{es}$. For most frequencies $\tau_T \gg 1$. In the spectral range where free-free opacity is the dominant absorption mechanism, yet $\kappa_{ff} < \kappa_{es}$, we define y_{ff} by

$$y_{ff} = 0.055 h_{13}^{2/3} T_5^{10/3} \frac{\omega^2}{(1 - e^{-\omega})^{2/3}} \quad (8)$$

where $\omega = h\nu/kT$, h_{13} is the scale height for changes in the gas density near the photosphere in 10^{13} cm and T_5 is the disk temperature in 10^5 K.

For our range of central masses and accretion rates, the height of the radiation pressure supported disk is $\lesssim 10^{14}$ cm. At $\Sigma \gtrsim 100$ gm/cm² gas pressure gradients support the disk against gravity and we find that the scale height is typically 10^{-3} times the thickness of the disk. The photosphere lies in the gas pressure supported layer of the disk for virtually

all frequencies in all our models, implying that $h_{13} \lesssim 10^{-2}$. The photospheric temperature is $T \lesssim 10^5$ K, and we conclude that $y_{ff} < 10^{-3}$ for all our models. Including bound-free opacity in this estimate would further reduce y_{ff} . Note, however, the very sharp dependence of y on temperature. Smaller central masses, which lead to higher temperatures, can create circumstances in which Comptonization is significant (e.g. as in the work of Ross *et al.* 1992).

Departures from LTE level populations become significant when the gas pressure in the disk is $P \lesssim 100$ dyn cm $^{-2}$ (Storzer, *et al.* 1994). When the gas pressure is this low, non-LTE effects can reduce the amplitude of the Lyman edge or drive it into emission. However, we expect LTE to be a good approximation in our case because $P \gtrsim 100$ dyn cm $^{-2}$ near the photospheres of our models. To check this assumption, we have made a non-LTE calculation of the disk spectrum for the case $m_8 = 2.7$ and $\dot{m} = 0.3$. As expected, we find that non-LTE effects have a negligible effect upon the spectrum.

4. Conclusion

We have calculated the vertical structure and UV spectrum of a conventional, viscously heated, accretion disk around a massive non-rotating black hole. Electron scattering dominates the opacity and the disk is supported by radiation pressure, except in the uppermost layers, where the gravitational acceleration becomes large and gas pressure gradients support the disk. The computed midplane density and temperature agree with the predictions of analytic calculations of the vertical structure (LN89, Shakura & Sunyaev 1973), if the Riffert & Herrold (1995) corrections to the vertical gravity are included.

Although the flux weighted mean opacity is dominated by electron scattering, the absorptive opacity can exceed the Thomson opacity both below the Lyman edge and above the HeII edge. In contrast, the best previous calculation (LN89) assumed that electron scattering dominates the opacity at all frequencies, leading them to overestimate the flux in these frequency ranges. As a consequence of our improved treatment of the gas opacity and radiative transfer, we find greater overall spectral curvature and larger features at the Lyman edge and the HeII edge. Although the spectral index of the near UV spectrum of the hotter disks is near the Newtonian black body value ($\alpha_n = 1/3$), this is just a coincidence. We find that the local black body approximation is not a good description of the disk spectrum.

We computed spectra assuming that the viscous stress was proportional to the total (gas plus radiation) pressure, the gas pressure and the geometric mean of the two pressures.

We find that the lower densities in the P_t case cause the flux above the HeII edge to increase by about an order of magnitude and the flux below the Lyman edge to decrease by about a factor of two. This results in somewhat smaller edge amplitudes in this case. The flux between these two energies is unaffected by the viscosity prescription.

The shape of the UV spectrum is determined by the effective temperature of the disk radiation or, equivalently, $\dot{m}m_8^{-1}$. For the hottest disks, the near UV spectral index, $\alpha_n \simeq 0.4$ and the far UV index, $\alpha_f \simeq -1.4$. The Lyman edge can be in emission for these disks. The coldest disks have softer near UV spectra ($\alpha_n \simeq -0.6$) and are completely absorbed above the Lyman edge.

The average optical-UV power-law index for quasars is ~ -0.5 (Laor 1990) but a single power law is a poor description of the continuum spectrum (Francis, *et al.* 1991). The continuum of the composite quasar spectrum, formed by combining all the quasars in the Large Bright Quasar Survey, softens with increasing frequency (Francis, *et al.* 1991). Both the mean optical-UV slope and the spectral curvature are consistent with our predicted UV spectrum of an irradiated disk if $\dot{m}m_8^{-1} \sim 10^{-3}$. However, disks this cold would be completely absorbed above the Lyman edge, which is not observed (Antonucci, Kinney & Ford 1989; Koratkar, Kinney & Bohlin 1992). On the other hand, disks hot enough to eliminate the Lyman edge feature all have α_n much larger than the observed slope.

Observational support for the existence of accretion disks in AGN originally came from the qualitative match between the “Big Blue Bump” and the characteristic temperature scale predicted by the thermal accretion disk model. We now see that the simplest theoretical models fail when confronted with more specific spectral tests. The model considered here, in which the dissipation all occurs inside a geometrically thin, but optically very thick, disk around a non-rotating black hole does not adequately explain the observed UV spectrum.

The next step in this program is to study the consequences of placing accretion disks around rotating (Kerr) black holes. Laor (1992) argued that the large Doppler shifts and gravitational redshifts of disk radiation from near the last stable orbit of a Kerr black hole could spread the Lyman edge feature and make it undetectable, but did not present detailed calculations of these effects. In addition, the effective temperature distribution for a disk around a Kerr black hole is different from that for a disk around a Schwarzschild hole, and this, too, may affect the shape of the UV continuum. We plan to construct models for the structure and UV continuum emission from disks around Kerr black holes in the near future.

We would like to thank Ari Laor for helpful conversations and for providing many

disk spectra. We also thank Omer Blaes and Eric Agol for ongoing conversations. MWS received support for this work from NASA grants NAGW-3129, 1583 and NAG 5-2925, and NSF grant AST 93-15133. JHK was partially supported by NASA Grant NAGW-3156.

REFERENCES

- Antonucci, R. R. J., A. L. Kinney & H. C. Ford 1989 *Ap. J.*, 342, 64
- Auer, L. H. & D. Mihalas 1970 *M.N.R.A.S.*, 149, 65
- Blaes, O.M. & E. Agol 1996 *Ap. J.*, 469, 41
- Dörrer, T., H. Riffert, R. Staubert & H. Ruder 1996 *Ast. Ap.*, 311, 69
- Francis, P. J., *et al.* 1991 *Ap. J.*, 373, 465
- Hubeny, I. & V. Hubeny, 1997, preprint
- Koratkar, A., A. L. Kinney & R. C. Bohlin 1992 *Ap. J.*, 400, 435
- Laor, A. & H. Netzer 1989 *M.N.R.A.S.*, 238, 897 (LN89)
- Laor, A., H. Netzer & T. Piran 1990 *M.N.R.A.S.*, 242, 560
- Laor, A. 1990 *M.N.R.A.S.*, 246, 369
- Laor, A. 1992, in *Testing the AGN Paradigm: AIP Conference Proceedings 254*, American Institute of Physics, New York
- Malkan, M. A. & W. L. W. Sargent 1982 *Ap. J.*, 254, 22
- Malkan, M. A. 1983 *Ap. J.*, 268, 582
- Mihalas, D. M., 1978, *Stellar Atmospheres*, W. H. Freeman & Co., San Francisco
- Novikov, I. & K. S. Thorne, 1973 in *Black Holes*, p. 422, eds: deWitt C. & B. deWitt, Gordon & Breach, New York
- Page, D. N. & K. S. Thorne 1974 *Ap. J.*, 191, 499
- Pringle, J.E. 1981 *Ann. Rev. Astr. Ap.*, 19, 137
- Riffert, H. & H. Herrold 1995 *Ap. J.*, 450, 508
- Rybicki, G. B. & A. P. Lightman, 1979, *Radiative Processes in Astrophysics*, John Wiley & Sons, Inc., New York
- Ross, R., A.C. Fabian & S. Mineshige 1992 *M.N.R.A.S.*, 258, 189
- Shakura, N. I. & R. A. Sunyaev 1973 *Ast. Ap.*, 24, 337
- Shakura, N. I. & R. A. Sunyaev 1976 *M.N.R.A.S.*, 175, 613

- Shields, G. A. 1978 *Nature*, 272,706
- Shimura, T. & F. Takahara 1993 *Ap. J.*, 419, 78
- Sincell, M.W. & J.H. Krolik 1997 *Ap. J.*, 476, 605 (SK97)
- Störzer, H., P.H. Hauschildt & F. Allard 1994 *Ap. J.*, 437, L91
- Sun, W.-H. and Malkan, M.A. 1989 *Ap. J.*, 346, 68

Figure and Table Captions

Figure 1. The density (a) and temperature (b) profiles for a standard accretion disk. Model parameters are $\dot{m} = 0.3$, $m_8 = 2.7$ and $r = 6.8$. The dashed line is the analytic model of LN89.

Figure 2. Comparison of the face-on disk spectra calculated by LN89 and in this paper. The disk parameters are $m_8 = 2.7$ and $\dot{m} = 0.3$.

Figure 3. The face-on standard disk spectrum for a fixed mass accretion rate and varying central mass.

Figure 4. The face-on standard disk spectrum for a fixed central mass and varying mass accretion rate.

Figure 5. The face-on standard disk spectrum as a function of viscosity prescription.

Table 1. Parameters of the UV spectra.

\dot{m}	m_8	\dot{m}/m_8	α_n	α_f	A_l
0.003	2.7	10^{-3}	-0.3	$-\infty$	0.0
0.03	0.27	10^{-1}	0.4	-1.4	0.9
0.03	2.7	10^{-2}	0.1	-3.2	0.6
0.03	27.0	10^{-3}	-0.6	$-\infty$	0.3
0.3	2.7	10^{-1}	0.2	-1.2	1.6

Table 1:

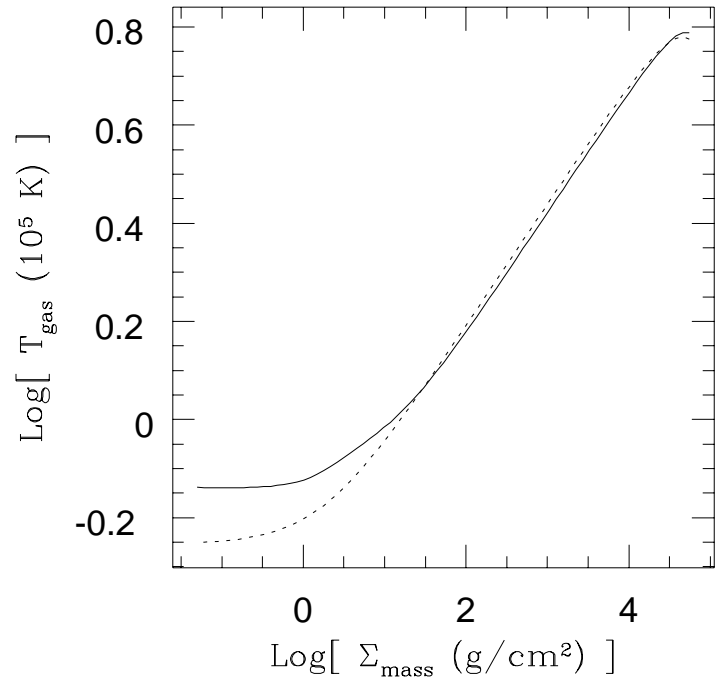
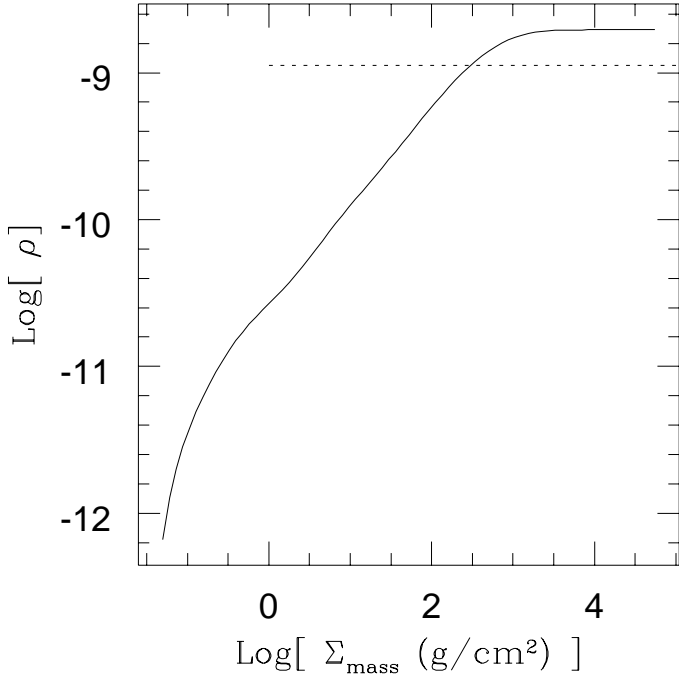


Fig. 1.—

Fig. 2.—

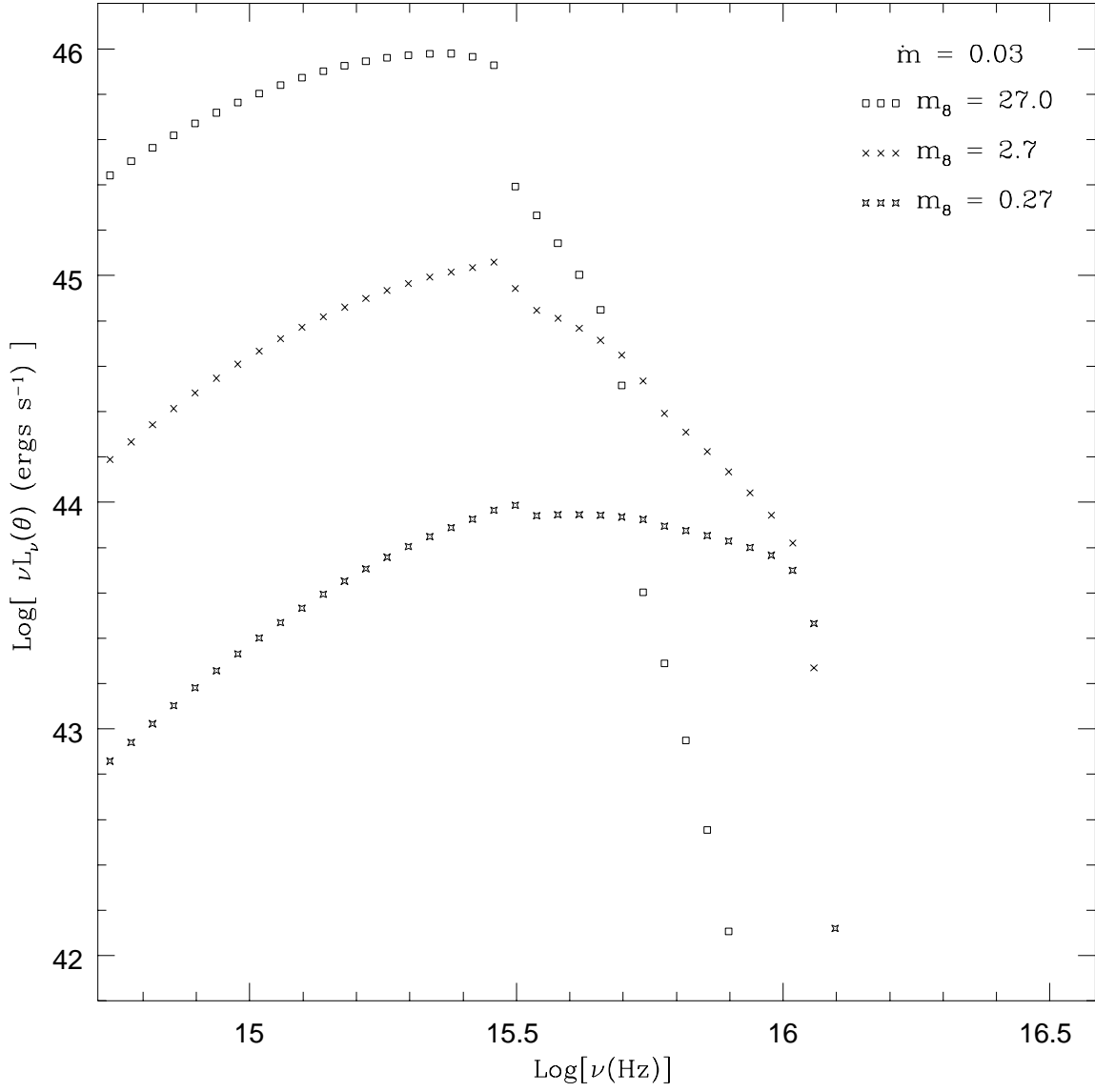


Fig. 3.—

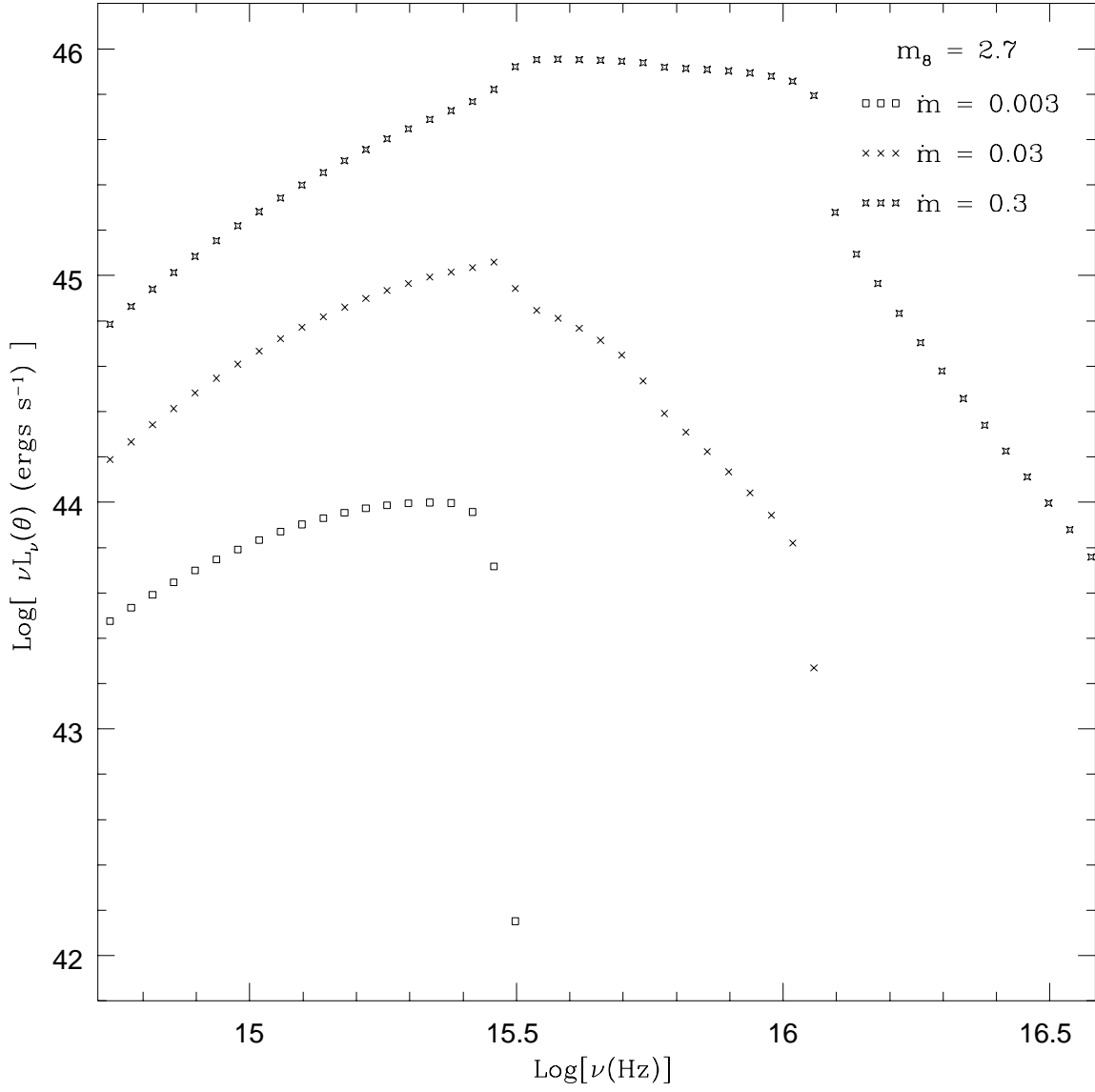


Fig. 4.—

Fig. 5.—